Effectiveness of Emission Controls on Atmospheric Oxidation and Air Pollutant Concentrations: Uncertainties due to Chemical Mechanisms and Inventories

Mingjie Kang[1,2], Hongliang Zhang[3], Qi Ying[4,a]

[1] School of Applied Meteorology, Nanjing University of Information Science and Technology. Nanjing 210044, China.

[2] Atmospheric Environment Center, Joint Laboratory for International Cooperation on Climate and Environmental Change, Ministry of Education, Nanjing University of Information Science and Technology. Nanjing 210044, China.

[3] Department of Environmental Science and Engineering, Fudan University, Shanghai 200433, China.

[4] Zachry Department of Civil and Environmental Engineering, Texas A&M University, College Station, Texas 77843-3136, USA.

[a] Currently at the Division of Environment and Sustainability, Hong Kong University of Science and Technology, Clear Water Bay, Kowloon, Hong Kong, China.

Correspondence to: Qi Ying (qying@ust.edu)(qying@ust.hk)

Abstract. In this study, three photochemical mechanisms of varying complexity from the Statewide Air Pollution Research Center (SAPRC) family and two widely used anthropogenic emission inventories are employed to quantify the discrepancies in the predicted effectiveness of nitrogen oxides (NO_x) and volatile organic compound (VOC) emission controls on ozone (O_3), secondary inorganic aerosols (SIA), and hydroxyl (OH) and nitrate (NO_3) radicals using the Community Multiscale Air Quality (CMAQ) model. For maximum daily average 8-hour O_3 (O_3-8h), relative reductions predicted using different emission inventory and mechanism combinations are consistent for up to 80% NO_x or VOC reductions, with maximum differences of approximately 15%. For ~~secondary inorganic aerosols (~~SIA~~),~~, while the predicted relative changes in their daily average concentrations due to NO_x reductions are quite similar, very large differences of up to 30% occur for VOC reductions. Sometimes even the direction of change (i.e., increase or decrease) is different. For the oxidants OH and NO_3 radicals, the uncertainties in the relative changes due to emission changes are even larger among different inventory-mechanism combinations, sometimes by as much as 200%. Our results suggest that while the O_3-8h responses to emission changes are not sensitive to the choice of chemical mechanism and emission inventories, using a single model and mechanism to evaluate the effectiveness of emission controls on SIA and atmospheric oxidation capacity may have large errors. For these species, the evaluation of the control strategies may require an ensemble approach with multiple inventories and mechanisms.

1. Introduction

Tropospheric ozone (O_3) pollution remains a major global concern. O_3 plays a critical role in atmospheric chemistry and is an important target for air quality improvement (Lu et al., 2018; Lyu et al., 2023; Real et al., 2024) because high levels of surface O_3 negatively affect human health, agricultural crop yields and plant growth (Du et al., 2024; Feng et al., 2022; Ghude et al., 2016; Lu et al., 2020; West et al., 2006). Surface O_3 is mainly formed by the photochemical reactions of NO_x and volatile organic compounds (VOCs) emitted from anthropogenic and biogenic sources (Finlayson-Pitts and Pitts Jr, 1999; Seinfeld and Pandis, 2016). The development of effective O_3 control strategies is hampered by the considerable spatial and temporal variability of surface O_3 concentrations and their non-linear relationship with emissions and meteorological conditions.

Three-dimensional chemical transport models (CTMs) are a valuable tool for developing effective air pollution control strategies. They can provide spatial and temporal information on O_3, particulate matter, and toxic air pollutants by numerically solving the mathematical equations describing the emission, reaction, transport, and deposition of primary and secondary atmospheric pollutants (Byun and Schere, 2006; Russell, 1997). The veracity of modeling outcomes is contingent upon the gas-phase chemical mechanisms and emission inventories, among other variables. Reliance on a single chemical mechanism and emission inventory may result in substantial uncertainty in modelled pollutant concentrations. A common approach to reduce uncertainty in air quality model predictions is to use an ensemble of simulations with different emission inventories and chemical mechanisms (Hu et al., 2017a).

Photochemical mechanism is one of the core components of all CTMs. While the representation of inorganic chemistry is generally similar across mechanisms, the representation of atmospheric organic chemistry differs significantly in terms of the number of explicit model species, the lumping schemes, and the radical chemistry, leading to variations in the model predictions of O_3, $PM_{2.5}$, air toxics, and some important radical species (Griffith et al., 2016; Kim et al., 2009). Furthermore, the responses of the predictions to changes in emissions may also differ depending on the photochemical mechanism employed, which may impact the assessment of emission control strategies. In practical applications, it is of the utmost importance to strike a balance between mechanism complexity and computational efficiency. For long-term modeling studies of criteria pollutants and the evaluation of numerous emission control strategies, condensed mechanisms may prove to be the optimal choice. More detailed mechanisms are appropriate for a broader range of applications, such as

72 investigations into specific reaction products that are not explicitly represented in condensed

73 mechanisms. However, they are more demanding on computational resources.

74   In this context, several mechanism comparison studies have been conducted. Differences

75 in predicted O_3 levels using various photochemical mechanisms have been reported (Yu et al.,

76 2010; Venecek et al., 2018). In addition to directly comparing the model predictions of O_3

77 concentrations, comparative analyses were also undertaken to examine the similarities and

78 differences between these mechanisms in predicting O_3 changes in response to changes in

79 precursor emissions. For example, Li et al. (2012) and Kang et al. (2022) compared several

80 mechanisms from the SAPRC family, including the standard versions of SAPRC-99, SAPRC-

81 07, SAPRC-11, and a highly condensed version of SAPRC-07. Their results showed that,

82 despite discrepancies in the predictions for O_3, key radicals such as OH and HO_2, and oxidation

83 products such as HNO_3, H_2O_2, NO_2, PAN, and HCHO, the relative changes in O_3 due to

84 changes in NO_x and VOC emissions were almost identical.

85   On the other hand, the accuracy of model predictions is also significantly affected by

86 uncertainties in anthropogenic emission inventories (Hu et al., 2017a; Kang et al., 2022; Placet

87 et al., 2000), which primarily arise from uncertainties and variability in activity levels (e.g.,

88 industrial production or energy consumption) and emission factors (Akimoto et al., 2006; Lei

89 et al., 2011; Streets et al., 2003). For example, when local speciation profiles are not available

90 for the generation of mechanism-specific VOC emissions from the emission rate of non-

91 methane hydrocarbons, average speciation profiles from the SPECIATE database developed

92 by the US EPA were often adopted (Bray et al., 2019; Li et al., 2014; Streets et al., 2003; Wu

93 and Xie, 2017). However, the emission factors from the SPECIATE profiles are predominantly

94 representative of the characteristics of local emissions, as a consequence of the disparities in

95 emission standards and control technologies among diverse geographical regions (Sha et al.,

96 2021). This introduces uncertainties into the emissions and the predicted pollutant

97 concentrations.

98   To date, several emission inventories covering China have been developed, such as the

99 Multi-resolution Emission Inventory for China (MEIC), the Regional Emission inventory in

100 ASia (REAS), and the Emission Database for Global Atmospheric Research (EDGAR). These

101 inventories have been successfully applied in chemical transport modeling to investigate the

102 concentration and spatial distribution of O_3 and other pollutants (Hu et al., 2017b; Kang et al.,

103 2021; Li et al., 2019, 2018; Saikawa et al., 2017; Xue et al., 2020; Yamaji et al., 2008). Hu et

104 al. (2017a) reported inconsistencies in emission inventories in predicting O_3 and $PM_{2.5}$ using

105 the Weather Research and Forecasting/Community Multiscale Air Quality (WRF/CMAQ)

106   model system. Ma et al. (2004) identified variations in NO_x and VOC emissions among

107   different inventories as the main factors influencing modeled O_3 concentrations. Our previous

108   study, which employed the condensed SAPRC-07 mechanism and two anthropogenic emission

109   inventories (MEIC and REAS), also observed relatively larger differences in O_3 predictions

110   between inventories in megacities of Beijing and Shanghai, especially on days with elevated

111   O_3 levels (Kang et al., 2022).

112   While several studies have explored the differences in model predictions due to varying

113   chemical mechanisms or emission inventories, a comprehensive analysis of the influence of

114   diverse combinations of these two factors on the sensitivity of O_3 and other air pollutants to

115   emission changes in China has yet to be undertaken. In this study, we address this gap by

116   applying the CMAQ model, integrated with three photochemical mechanisms and two widely

117   used emission inventories, to quantify the effects of different combinations of mechanisms and

118   inventories on the predictions of maximum daily average 8-hour ozone (O_3-8h) and other

119   secondary pollutants in different regions of China. In addition, the impacts on atmospheric

120   oxidation capacity and key gaseous pollutants are investigated. To gain insight into the

121   variations in pollutant sensitivity, a series of incremental emission reduction scenarios were

122   used, thereby enabling the quantification of the influence of different mechanism and inventory

123   combinations on the response of O_3 and related pollutants. The findings of this study can assist

124   policymakers in the development of more effective and adaptive pollution control strategies.

125

126   **2. Materials and methods**

127   **2.1 The CS07, SAPRC-11 and SAPRC-18 mechanisms**

128   The SAPRC mechanism is a widely used photochemical mechanism that represents complex

129   atmospheric reactions in computationally tractable forms. Instead of tracking the oxidation of

130   individual precursor organic compounds and their reaction products explicitly, the SAPRC is

131   a lumped-molecule chemical mechanism that groups structurally similar VOC species (e.g.,

132   alkanes, akenes, and aromatics) into several groups of lumped model species. Some important

133   species, such as isoprene and formaldehyde, are represented explicitly. The reactions of each

134   lumped model species with common oxidants (OH, NO_3 and O_3) are derived based on the

135   reactions of individual species within that group, which are generated automatically using a

136   mechanism generator (Carter et al., 2025). One of the complexities in representing VOC

137   reactions is the intermediate oxidation products and radical species. In the SAPRC mechanism,

138   the radicals such as peroxyl radicals and intermediate products such as organic nitrates are

139 represented by a group of common species to reduce the number of reactions and model species.

140 A brief comparison of the three SAPRC mechanisms is summarized in Table S1.

141 Three different chemical mechanisms from the SAPRC mechanism family were used in

142 this study, i.e., the condensed SAPRC-07 (CS07) (Carter, 2010), the standard SAPRC-11 (S11)

143 (Carter and Heo, 2013), and the standard SAPRC-18 (S18) (Carter, 2020). These mechanisms

144 were selected to represent different levels of detail in gas-phase reactions in a regional chemical

145 transport model. The CS07 was derived from the widely used SAPRC-07 mechanism and has

146 a high condensation level similar to that of the Carbon Bond mechanism, which is also widely

147 used. The S11 is an updated version of the SAPRC-07 mechanism, with significant revisions

148 made to the aromatic chemistry. The S11 mechanism employed in this study is identical to that

149 utilized in our previous study (Kang et al., 2021). For a detailed description of CS07 and S11

150 regarding O_3 source apportionment and emission sensitivity, please refer to Kang et al. (2022).

151 The S18 mechanism represents a complete update of the SAPRC mechanism since SAPRC-07.

152 S18 incorporates a greater number of model species, a more explicit representation of peroxyl

153 radical chemistry, and a lumping scheme that is more suitable for predicting secondary organic

154 aerosol (SOA) formation. Due to these modifications, S18 is more extensive than S11 in terms

155 of both the number of species and chemical reactions. Although it has been successfully applied

156 in photochemical box models (Jiang et al., 2020; Li et al., 2022a, b), it has not yet been

157 implemented in 3D regional CTMs.

158

159 **2.2. Anthropogenic emission inventories**

160 The present study compares two widely used anthropogenic emission inventories, MEIC

161 (http://www.meicmodel.org) and REAS 3.1 (https://www.nies.go.jp/REAS/), to investigate O_3

162 pollution in China. The emission data from these inventories were processed using an in-house

163 emission processor. Detailed VOC speciation profiles selected from the US EPA-developed

164 SPECIATE database were processed using the speciation profile processor from W.P.L. Carter

165 (2015) to generate profiles for the CS07, SAPRC-11, and SAPRC-18 mechanisms, which are

166 used to estimate emissions of CMAQ-ready VOCs. The MEIC emission inventory includes

167 only emission estimates in China, whereas the REAS emission inventory has complete spatial

168 coverage for Asian countries. In the MEIC simulation, emissions from other countries are

169 supplemented using data from the REAS inventory.

170

171 **2.3 Model application**

172   The CS07, S11, and S18 mechanisms were incorporated into the CMAQ model (version 5.0.2)

173   to evaluate the differences of mechanisms and inventories in predicting O_3-8h, OH and NO_3

174   radicals, secondary inorganic aerosols, and reactive VOC species (HCHO) in July 2017 in

175   China. July is widely used in modeling studies to represent conditions of a typical summer

176   month (Kang et al., 2021). The model domain, which covers China and surrounding areas in

177   eastern and southeastern Asia at a 36 km × 36 km horizontal resolution, along with the locations

178   of cities mentioned in the manuscript, is illustrated in Figure S1.

179   The simulations included model runs with the following combinations: S11 mechanism

180   with MEIC inventory (S11-MEIC), S11 with REAS (S11-REAS), CS07 with MEIC (CS07-

181   MEIC), CS07 with REAS (CS07-REAS), and S18 with REAS (S18-REAS). The MEIC only

182   has five emission sectors, making it difficult to re-speciate the emissions for the S18

183   mechanism. Specifically, solvent utilization emissions are not represented in the public version

184   of MEIC as a separate sector (Wang et al., 2018). Since solvent utilization accounts for a

185   significant fraction of VOC emissions in urban areas and has very different emission

186   characteristics than fuel combustion sources, re-speciating the five-sector MEIC VOC

187   emissions will be inaccurate. It should be noted that while the MEIC emission inventory is for

188   2017, the most recent year in the REAS inventory is 2015, which is the one used in the current

189   study.

190   The July anthropogenic emission inventories from MEIC and REAS were processed using

191   an in-house emission processor, with updated speciation profiles employed to generate CMAQ-

192   ready VOC emissions (Kang et al., 2022). The speciation profiles for different chemical

193   mechanisms were derived from the same detailed speciation profiles extracted from the

194   SPECIATE database. Comprehensive overviews of MEIC and REAS inventories were

195   provided by Kang et al. (2022). Comparisons of major species, including NO_x ($NO+NO_2$), SO_2,

196   ethene (ETHENE), formaldehyde (HCHO), higher olefins (OLE) (comprising OLE1 and

197   OLE2, which are lumped alkene species with propylene and trans-2-pentene as representative

198   compounds), isoprene (ISOPRENE), and monoterpenes (TRP1), are shown in Tables S2-S3

199   and Figures S2-S3 for municipalities and provinces in July 2017. Note that OLE and TRP1

200   emissions are ~~for~~from the S11 mechanisms. Emissions for CS07 are similar but some of the

201   species in OLE and TRP1 are explicit species in S18. There are notable spatial differences in

202   the weekday emissions of HCHO, ETHENE, OLE, SO_2, and NO_x between MEIC and REAS.

203   Specifically, REAS exhibits higher HCHO emissions in locations like Beijing, Tianjin, Henan,

204   Shanghai, and Guangzhou than MEIC (Figure S2). In the south of Henan, ethene emissions are

significantly higher in REAS relative to MEIC. The emissions of OLE in REAS are lower than those in MEIC in Beijing, Tianjin, Shanghai, Guangzhou, Chengdu, and Chongqing. SO_2 emissions in MEIC are generally lower than those in REAS, except for Shanghai and Guangzhou. NO_x emissions differ significantly between MEIC and REAS. In eastern China, including cities like Shanghai and Guangzhou, NO_x emissions from REAS are typically lower than those from MEIC, although some areas demonstrate a notable increase. These discrepancies inevitably affect the accuracy of air pollutant predictions, underscoring the necessity for a comprehensive assessment of emission inventories in the development of effective pollution control ~~polices~~policies.

Biogenic emissions were generated using the Model of Emissions of Gases and Aerosols from Nature (MEGAN) version 2.10, which has been observed to emit higher levels of isoprene and monoterpenes in comparison to anthropogenic sources (Figure S3). Open burning emissions were produced using FINN inventory from the National Center for Atmospheric Research (NCAR) (Wiedinmyer et al., 2011). Sea salt and windblown dust emissions were simulated online using the CMAQ model. Initial and boundary conditions for the model simulation were generated using CMAQ default profiles. The initial three days of the simulation serve as a spin-up and are excluded from subsequent analyses.

Meteorological inputs were generated using the Weather Research and Forecasting (WRF) model version 4.2 for the 36×36 km domain with 44 vertical layers. The initial and boundary conditions for WRF were derived from the global reanalysis data FNL (available at https://rda.ucar.edu/datasets/ds083.2/). Further details on the configuration of WRF model can be found in the work of Kang et al. (2022). WRF-derived meteorological parameters, including temperature and relative humidity at a height of 2 m above the surface and wind speed and direction at 10 m, have been validated against observational data from the National Climatic Data Center (NCDC), demonstrating good performance (Kang et al., 2021).

2.4 Sensitivity of O_3 and related pollutants to emission controls across different mechanisms and inventories

A large number of sensitivity simulations with systematic reductions in NO_x and VOC emissions were conducted to explore variations in the sensitivity of O_3-8h and related pollutants to emission reductions across different mechanisms and inventories. Three sets of simulations were performed for each mechanism/inventory combination considered in this study (see section 2.3). In the first set of simulations, NO_x emissions were reduced by 20, 40,

238 50, 60, and 80%, while the emissions of VOCs were maintained at their base-case level. In the

239 second set of simulations, VOC emissions were reduced by 20, 40, 50, 60, and 80%, while NO_x

240 emissions remained constant. In the third set of simulations, both NO_x and VOC emissions

241 were reduced by 20, 40, 50, 60, and 80%.

242

243 **3. Results and discussion**

244 **3.1 Model evaluation of O_3 and $PM_{2.5}$ predictions across various mechanisms and**

245 **inventories**

246 Observations of O_3-8h and $PM_{2.5}$ at a large number of surface monitoring stations nationwide

247 in July 2017 were obtained from the publication website of the China National Environmental

248 Monitoring Center (http://www.cnemc.cn). The model performance statistics were evaluated

249 separately for different regions: the North China Plain (NCP), Yangtze River Delta (YRD),

250 Central China (Center), Pearl River Delta (PRD), and Sichuan Basin (SCB). Specifically, NCP

251 includes Beijing, Tianjin, and some cities in Hebei and Shandong provinces; Center includes

252 cities in the provinces of Henan, Hubei, Hunan, and Jiangxi; YRD includes Shanghai and some

253 cities in the provinces of Anhui, Jiangsu, and Zhejiang; PRD includes Shenzhen and some

254 cities in Guangdong province; and SCB includes Chongqing and some cities in Sichuan

255 province. As shown in Figures S4-S5, the model performance for O_3-8h and $PM_{2.5}$ predicted

256 by different mechanisms and emission inventories in major regions of China exhibits large

257 variations, due to differences in climate, topography, and emission sources. Overall, the

258 average values of mean normalized bias (MNB) and mean normalized error (MNE) for O_3-8h

259 predictions across all combinations of mechanisms and inventories are generally within the

260 ~~model performance criteria suggested by the US EPA~~recommended model performance

261 criteria (MNB≤±0.15 and MNE≤0.3) (Emery et al., 2017) in most regions, except for

262 underprediction in the PRD. Similarly, the model shows good performance for $PM_{2.5}$ in most

263 areas, except for the PRD region, where the mean fractional biases (MFB) for $PM_{2.5}$ using S18-

264 REAS, CS07-REAS, and S11-REAS are slightly outside the recommended range (Boylan and

265 Russell, 2006). The underestimation of $PM_{2.5}$ predictions using REAS in the PRD, as shown

266 in Figure S5, is likely related to biases in this inventory specific to this region.

267

268 **3.2 Spatial variations in predictions of O_3 and related pollutants by different mechanisms**

269 **and inventories**

270 Figure 1 shows the spatial distribution of monthly averaged O_3-8h concentrations predicted by

271 S11-MEIC in July, along with the absolute differences between O_3-8h predictions from S11-

MEIC and those from other mechanisms and inventories. Based on S11-MEIC, high O_3-8h levels exceeding 80 ppb occurred in eastern China, especially in Beijing, Tianjin, Hebei, northern Henan, SCB, and Shanghai. Extremely high O_3-8h levels above 100 ppb are also observed over the Bohai Bay and the Yellow Sea, likely due to regional transport of polluted air from the continent, reduced NO_x titration with O_3, and lower O_3 dry deposition velocities over the ocean. (Luhar et al., 2017; Silva and Heald, 2018). Similar spatial distributions of O_3-8h concentrations are also found in the simulations using other mechanisms and inventories (Figure S6). In comparison, O_3-8h concentrations predicted by S11-REAS are generally 2–7 ppb higher than those by S11-MEIC in most parts of China, especially in the central region, Zhejiang, and Fujian provinces, but about 2–7 ppb lower in Beijing, Shanghai, Chengdu, and the PRD region. S18-REAS predicted significantly lower O_3-8h levels, with reductions greater than 7 ppb in regions such as Beijing, Tianjin, Hebei, Shanghai, SCB, PRD, and other developed areas such as Zhengzhou and Hefei.

In contrast, CS07-MEIC predicted lower O_3-8h levels overall, with apparent reductions of ~ 6–7 ppb in the SCB, central China, and coastal areas near Shanghai. Similarly, CS07-REAS also showed generally lower O_3-8h concentrations compared to S11-MEIC, particularly in Chengdu, Luoyang, Shanghai, Guangzhou, Ningbo, Hefei, Nanchang, and the Yellow Sea (~7 ppb lower or more), although some locations exhibit higher O_3-8h levels than those predicted by S11-MEIC. These discrepancies highlight that the accuracy of O_3 predictions is sensitive to variations in photochemical mechanisms and emission inventories. This underscores the importance of adopting and comparing multiple mechanisms and inventories when developing region-specific pollution control policies.

The difference in Figure 1(c) for other countries is mainly due to the difference between S11 and S18. Predicted O_3 concentrations by S18 are lower than those by S11, especially in urban areas (e.g., in Ulaanbaatar in Mongolia). This is consistent with the box-model simulation results reported by Carter (Carter, 2020). In Figure 1(a), the difference of the monthly O_3 in other countries is negligible when the same chemical mechanism is used, which further confirms our conclusion.

In Figures 1(b), O_3 concentrations from S11-REAS are significantly lower than those from S11-MEIC. This is because O_3 formation sensitivity regime over the yellow sea is likely NO_x-limited as the VOC-sensitive urban plume is advected to the marine environment (Vermeuel et al., 2019). Furthermore, satellite observed HCHO/NO_x columns over the Yellow Sea is greater than 6, clearly indicating a NO_x-limit regime (Kang et al., 2021). Since the NO_x emissions in the upwind regions in the REAS inventory are significantly lower than

306 these in the MEIC inventory, this leads to reduced O_3 formation in the S11-REAS results

307 compared to the S11-MEIC results.

308   Figure 2 illustrates the differences in spatial distribution of monthly averaged secondary

309 inorganic aerosol (SIA) concentrations modeled with different mechanisms and inventories.

310 According to S11-MEIC, high SIA concentrations are mainly concentrated in NCP and SCB,

311 exceeding 15 μg m^{-3}. High SIA concentrations are also found in Bohai Bay, likely due to long-

312 range transport of polluted air from land sources. Compared to S11-MEIC, S11-REAS predicts

313 higher SIA concentrations in most regions, with increases of > 1 μg m^{-3} in most areas,

314 especially in NCP, Henan, and SCB (higher by about 6 μg m^{-3} or even more). Nationwide, SIA

315 concentrations predicted by S18-REAS are generally higher than those predicted by S11-MEIC,

316 with increases of up to 6 μg m^{-3} or more in the NCP, Central China, SCB, Bohai Bay, and the

317 Yellow Sea. CS07-MEIC shows similar SIA levels to S11-MEIC, with slightly lower

318 concentrations of ~1 μg m^{-3} in SCB and Bohai Bay. The spatial differences in SIA predictions

319 between CS07-REAS and S11-MEIC are similar to those between S11-REAS and S11-MEIC,

320 suggesting that SIA concentrations from CS07-REAS and S11-REAS are comparable.

321

322 **3.3 Impacts of mechanisms and inventories on predicted atmospheric oxidation capacity**

323 Atmospheric oxidation capacity (AOC), which governs the removal rate of primary pollutants

324 and the production of secondary pollutants (Elshorbany et al., 2009; Prinn, 2003), is primarily

325 controlled by the hydroxyl (OH) and nitrate (NO_3) radicals in the atmosphere (Geyer et al.,

326 2001; Liu et al., 2022). The spatial differences in OH and NO_3 predictions for different

327 mechanisms and inventories are illustrated in Figures 3-4.

328   S11-MEIC predicts high OH concentrations exceeding 3.7×10^6 molecules cm^{-3} (0.15 ppt)

329 mainly in northern China, including NCP, Inner Mongolia, and some western sites. Compared

330 to S11-MEIC, S11-REAS predicts lower OH concentrations in NCP, Jiangsu, Shanghai, PRD,

331 SCB, and other urban nuclei but higher concentrations in rural areas. In contrast, S18-REAS

332 predicts higher OH concentrations than S11-MEIC in most regions, except in some northern

333 locations. CS07-MEIC produces elevated OH concentrations in northwestern China, Chengdu,

334 Chongqing, Shanghai, Hebei, Shandong, and northern Henan, but lower OH levels in other

335 regions. Similar to S11-REAS, CS07-REAS shows much higher OH levels in northwestern

336 China but lower OH levels in eastern regions than S11-MEIC. The variability in OH levels can

337 significantly affect the formation of O_3 and other gaseous and particulate pollutants.

The spatial distribution of NO_3 concentrations modeled by S11-MEIC exhibits high values in Xinjiang, Inner Mongolia, NCP, and Bohai Bay, with NO_3 concentrations reaching up to 20 ppt. Obvious differences in NO_3 predictions between S11-REAS and S11-MEIC are primarily observed in Xinjiang and Inner Mongolia, with smaller differences in other regions. S18-REAS generally predicted higher NO_3 concentrations than S11-MEIC, especially in Xinjiang, Inner Mongolia, Bohai Bay, Yellow Sea, and Taiwan Strait, by ~6 ppt or more. In contrast, CS07-MEIC consistently predicts lower NO_3 levels than S11-MEIC. CS07-REAS predicted lower NO_3 concentrations in the eastern regions but higher concentrations in parts of Xinjiang compared to S11-MEIC.

3.4 Impacts of mechanisms and inventories on HCHO prediction

Spatial variations in AOC, as reflected in OH and NO_3 predictions from different mechanisms and inventories, imply that photochemical formation and loss rates for air toxics may also vary depending on the mechanism and inventory used. To explore how these variations affect the modeling results for gaseous pollutants, we examined HCHO, one of the most important gaseous air toxics with both primary and secondary sources. It is also a significant contributor to O_3 formation and OH production, thus playing a crucial role in tropospheric photochemistry (Wang et al., 2017; Zhang et al., 2013).

~~HCHO concentrations predicted by S11-MEIC~~Monthly average surface HCHO concentrations from S11-MEIC are similar to the surface observations made in China (Zhang et al., 2021). HCHO concentrations are generally high in the SCB and eastern China, areas with significant biogenic VOC emissions ~~(Kang et al., 2023), particularly in Chengdu, Shanghai, and Changsha, where HCHO concentrations reach or exceed 7 ppb (Figure 5).~~(Kang et al., 2023a), particularly in Chengdu, Shanghai, and Changsha, where HCHO concentrations reach or exceed 7 ppb (Figure 5). This suggests that a significant fraction of the HCHO is due to secondary formation. HCHO levels predicted by S11-REAS are similar to those predicted by S11-MEIC, with only minor differences of less than 1 ppb. In contrast, S18-REAS predicts significantly lower HCHO levels than S11-MEIC, with differences > 1 ppb, especially in SCB, NCP, PRD, YRD, and central China. CS07-MEIC and CS07-REAS predict higher HCHO levels than S11-MEIC, especially in SCB and eastern China, with differences exceeding 1 ppb. These results indicate that HCHO predictions are more strongly influenced by photochemical mechanisms than by uncertainties in emission inventories, due to its secondary formation.

3.5 Impacts of mechanisms and inventories on the sensitivity of O_3 and related pollutants to emission controls

Figures 6-10 and S6-S15 display the fractional changes in predictions of O_3 and related pollutants due to NO_x and VOC reductions using various mechanisms and inventories.

3.5.1 Impacts of mechanisms and inventories on O_3 sensitivity to emission controls

For all mechanisms and inventories, O_3-8h concentrations consistently decrease with reductions in NO_x, VOCs, or both in all five cities in July. The efficiency of emission controls improves with increasingly higher emission reductions of NO_x, VOCs. These trends are consistent with the findings of Kang et al. (2021), suggesting that the mechanisms and inventories do not affect the trend of change in O_3, but do affect the magnitude of the change. These results also show that in July, the sensitivity of O_3 formation to NO_x and VOCs is in transition or NO_x-limited regimes. In Beijing, when NO_x emissions are reduced, CS07-MEIC and CS07-REAS show the largest O_3-8h reductions compared to other mechanisms and inventories, while S18-REAS exhibits the smallest changes, especially with larger NO_x reductions. In Shanghai, the largest O_3-8h reductions due to NO_x controls are observed with CS07-REAS, followed by S11-REAS, while S18-REAS again shows the smallest changes. In Changsha, there are no significant differences among mechanisms and inventories in the sensitivity tests. In Shenzhen, S11-REAS shows the greatest decreases in O_3-8h, followed by CS07-REAS and S18-REAS, while S11-MEIC and CS07-MEIC show the smallest changes. Except for S18-REAS, predictions from other mechanisms and inventories are similar in Chongqing.

When only VOC emissions are reduced in Beijing, S11-MEIC predicts the largest O_3-8h reductions, while CS07-REAS predicts the smallest changes. Similar patterns are found in Shanghai and Changsha, with larger differences among different mechanisms and inventories in Shanghai. In Shenzhen, S11-MEIC also exhibits the largest O_3-8h decreases, followed by CS07-MEIC, while CS07-REAS, S11-REAS, and S18-REAS show smaller changes. In Chongqing, S18-REAS predicts the largest changes and CS07-MEIC the smallest, although the differences among these scenarios are not substantial. When both NO_x and VOC emissions are reduced, the predicted change rates of O_3-8h do not vary much across different mechanisms and emission inventories for all five cities. Additionally, the sensitivity tests for Shenzhen, as presented in Figure 6, suggest that differences in emission inventories may have a greater impact on emission control outcomes than differences in chemical mechanisms. O_3 in Shenzhen is lower than other cities included in Figure 6 and most O_3 there is background O_3

404 on typical days (Kang et al., 2023b). Thus, it is less responsive to emission reductions than
405 other cities.

406   Figure S6 illustrates the national-scale relative changes in O_3-8h due to NO_x emission
407 reductions evaluated using different mechanisms and inventories. The results are consistent
408 with those shown in Figure 6, with the greatest O_3-8h reductions occurring in the SCB, Central,
409 and YRD. For all mechanisms and inventories, increasingly higher NO_x reductions generally
410 lead to increasingly lower O_3 in July, with relative changes in O_3-8h ranging from
411 approximately 5% to 60% as NO_x reductions increase from 20% to 80%. In comparison, the
412 O_3-8h reductions predicted by S18-REAS are less pronounced than other mechanisms and
413 inventories in most areas. Similar to NO_x reductions, higher VOC reductions typically result
414 in larger O_3 reductions in July, with significant reductions observed in NCP, Chengdu, PRD,
415 Shanghai, and Bohai Bay. The relative changes in O_3-8h increase from 5% to 40% as VOC
416 reductions increase from 20% to 80% in these areas (Figure S7). The comparison between
417 Figure S6 and Figure S7 suggests that NO_x reduction tends to be more effective in controlling
418 O_3 pollution in non-VOC-limited regions than VOC reduction, given the same level of
419 emission reduction.

420

3.5.2 Impacts of mechanisms and inventories on SIA sensitivity to emission controls
422 Reducing NO_x emissions typically leads to decreasing SIA levels across the five cities, with
423 the efficiency of reductions improving as NO_x reduction increases. As illustrated in Figure 7,
424 the predicted changes in SIA are quite similar for different mechanisms and inventories.
425 However, VOC controls do not always effectively reduce SIA concentrations, likely
426 attributable to an increase in NO_3 radicals, as shown in Figure 9. In Beijing, changes in SIA in
427 response to VOC reductions vary with mechanisms and inventories. For S11-MEIC and CS07-
428 MEIC, SIA concentration first increases and then decreases with decreasing VOCs. S18-REAS
429 shows a general decrease in SIA concentrations with decreasing VOCs. In contrast, CS07-
430 REAS and S11-REAS predict an increase in SIA concentrations with VOC reductions, with
431 the rate of SIA growth initially increasing and then decreasing as VOC emission decreases. In
432 Shanghai, VOC reductions generally increase SIA concentrations across all mechanisms and
433 inventories, especially for CS07-REAS and S11-REAS, which show that SIA concentrations
434 consistently increase as VOCs are progressively reduced. In Changsha, SIA concentrations also
435 consistently increase with increasing VOC reductions for all mechanisms and inventories. In
436 Shenzhen, SIA concentrations increase with VOC reductions; however, the changes are more
437 pronounced for S11-REAS compared to the less significant variations observed for CS07-

438 MEIC. Except for S18-REAS, Chongqing shows an increase in SIA concentrations with VOC

439 reductions, particularly for CS07-REAS. Overall, simultaneous reductions in NO_x and VOCs

440 decrease SIA levels in most cities, similar to the effects of NO_x controls alone.

441 Figure S8 shows the relative changes in SIA due to NO_x controls on a national scale, using

442 different mechanisms and inventories. The stepwise reductions in NO_x emissions lead to an

443 overall decrease in SIA concentrations, with the most pronounced reductions observed in the

444 NCP, SCB, Jiangsu, Bohai Bay, and Yellow Sea. The decreases in SIA increase from ~5% to

445 60% as NO_x reduction increases from 20% to 80%. On the contrary, VOC reduction causes an

446 overall increase in SIA concentrations (Figure S9), indicating that VOC controls are less

447 effective than NO_x controls in reducing SIA levels in July. Notably, the largest increases in

448 SIA are seen in SCB, Central, and YRD, where SIA increases grow from ~ 6% to 30% as VOC

449 reduction increases from 20% to 80%. In comparison, S18-REAS shows relatively smaller

450 changes in SIA, with some areas in NCP showing obvious decreases in SIA concentrations.

451

452 **3.5.3 Impacts of mechanisms and inventories on OH and NO_3 sensitivity**

453 As shown in Figures 8-9, the effects of NO_x reductions on OH concentrations vary depending

454 on the mechanism and inventory used. In most regions, OH production decreases with reducing

455 NO_x emissions, likely due to the decrease in O_3 concentrations, as O_3 photolysis in the presence

456 of water vapor is a significant source of atmospheric OH (Seinfeld and Pandis, 2016). Except

457 for Shenzhen, CS07-MEIC and CS07-REAS predict the largest decreases in OH due to NO_x

458 control in other cities, while S18-REAS predicts the smallest OH change rates. In Shenzhen,

459 OH levels predicted by S11-MEIC and CS07-MEIC initially increase and then decrease as NO_x

460 emissions decrease, while those predicted by S18-REAS, CS07-REAS, and S11-REAS exhibit

461 a consistent decrease in OH levels. When only VOCs are reduced, the changes in OH vary

462 across different mechanisms and inventories. In Beijing, except for S18-REAS, OH

463 concentration initially increases and then decreases with decreasing VOC emissions. In

464 Shanghai, OH concentrations from CS07-REAS and S11-REAS basically increase with

465 decreasing VOCs, while those from CS07-MEIC and S11-MEIC show an initial increase

466 followed by a decrease. S18-REAS predicts a general decrease of OH with decreasing VOCs

467 in Beijing and Shanghai. In Changsha, OH concentrations consistently increase with reduced

468 VOCs across all mechanisms and inventories, with CS07-REAS showing a rapid increase of

469 up to 75%. In Shenzhen, OH levels from CS07-REAS, S11-REAS, and S18-REAS increase

470 with decreasing VOCs, while those from S11-MEIC and CS07-MEIC decrease. In Chongqing,

471 all mechanisms and inventories except S18-REAS predict an increase in OH concentrations

with decreasing VOCs, with CS07-MEIC showing a significant increase of up to 75%. When both NO_x and VOC emissions are reduced, OH concentrations generally increase for all mechanisms and inventories, although the relative changes are relatively small (< 25%).

Figures S10-S11 display the spatial distribution of OH changes due to incremental emission controls across different mechanisms and inventories. There is a nationwide decrease in OH concentrations due to NO_x reductions, with more pronounced decreases in central and eastern China, where OH levels drop by ~ 20% to 80% as NO_x reduction increases from 20% to 80%. ~~Instead, VOC reductions generally lead to increased OH concentrations across most of China, significantly in some regions with large vegetation cover (Kang et al., 2023), such as central and southeastern China.~~ Instead, VOC reductions generally lead to increased OH concentrations across most of China, significantly in some regions with large vegetation cover (Kang et al., 2023a), such as central and southeastern China. In these areas, OH levels increase by 20~200% in response to stepwise VOC reductions. This increase occurs because high atmospheric VOC concentrations in rural and vegetation-rich areas react with OH radicals to produce RO_2 and HO_2, depleting OH, thus reducing VOCs in these areas increases OH levels. However, in some urban centers, such as Beijing and Shanghai, changes in OH levels due to VOC controls depend on the extent of reduction and the choice of mechanism and inventory.

Similar to OH, NO_3 levels predicted by different mechanisms and inventories basically decrease with decreasing NO_x emissions, likely related to the decline of O_3 concentrations since NO_3 radicals are predominantly formed by the reaction of NO_2 with O_3 (Geyer et al., 2001). In general, the change rates of NO_3 due to NO_x reductions are higher for CS07-MEIC and CS07-REAS, while lower for S18-REAS. When VOC emissions are reduced, NO_3 production increases, except for S18-REAS. In Changsha, a particularly dramatic increase of over 200% and 150% is observed for CS07-REAS and CS07-MEIC, respectively, when VOC emissions are cut by 80%. This increase in NO_3 radicals could be attributed to a decline in the rapid reaction of NO_3 with unsaturated hydrocarbons. However, for S18-REAS, NO_3 concentrations decrease with decreasing VOCs in Beijing, Shanghai, and Chongqing. Unlike OH, simultaneous reductions in NO_x and VOCs result in lower NO_3 levels across all mechanisms and inventories.

Figures S12-13 illustrate the spatial variation in NO_3 changes due to systematic emission reductions for all mechanisms and inventories. NO_3 radicals show a decreasing trend, particularly in eastern China, where reductions in NO_3 levels vary from 40% to 100%. Except for S18-REAS, other mechanisms and inventories generally predict a nationwide increase in NO_3 radicals with reduced VOCs, particularly in central and southeastern China, where NO_3

506 levels increase by ~ 30 – 300% or even more with increasing VOC reductions. S18-REAS

507 predicts a decrease in NO_3 levels with reduced VOCs in some megacities such as Beijing,

508 Shanghai, Chengdu, and Chongqing, while NO_3 levels increase elsewhere.

509

510 **3.5.4 Impacts of mechanisms and inventories on the sensitivity of secondary gaseous**

511 **pollutants to emission controls**

512 As shown in Figure 10, HCHO concentrations decrease with decreasing NO_x emissions, likely

513 due to decreased AOC, as evidenced by decreased OH and NO_3 levels. This indicates that

514 secondary formation from the oxidation of atmospheric VOCs is the dominant source of HCHO,

515 in accordance with previous studies (Wang et al., 2017; Yang et al., 2019; Zhang et al., 2013).

516 In addition, the most significant decreases in HCHO levels due to NO_x reductions are observed

517 for CS07-REAS in all five cities, particularly in Changsha and Chongqing, where HCHO levels

518 drop by about 40%. When VOCs are reduced alone, HCHO levels decrease linearly across all

519 mechanisms and inventories, a trend similar to the simultaneous reduction of NO_x and VOCs.

520 Variations in HCHO changes across different mechanisms and inventories suggest the need to

521 evaluate different mechanisms and inventories when formulating regional emission control

522 policies for carbonyl pollution.

523 Figures S14- S15 illustrate the spatial distribution of relative changes in HCHO due to NO_x

524 and VOC controls using different mechanisms and inventories. VOC and NO_x controls lead to

525 reductions in HCHO concentration, especially in eastern China. However, VOC controls

526 generally ~~leads~~lead to larger reductions in HCHO concentrations (~10–80%) than NO_x controls

527 (~ 4 – 40%), as shown in Figures S14-15 and 10. This suggests that VOC controls are also

528 essential and more effective for reducing secondary gaseous organic pollutants in the

529 atmosphere.

530

531 **4. Conclusions**

532 This study utilized the CMAQ model to evaluate the impacts of different mechanisms and

533 inventories on the prediction of O_3 and other air pollutants. It also examined how these

534 mechanisms and inventories affect the sensitivity of O_3 and related species to emission

535 reductions. For ~~maximum daily average 8-hour O_3 (~~O_3-8h~~)~~, relative reductions predicted using

536 different emission inventory and mechanism combinations are consistent for up to 80% NO_x

537 or VOC reductions, with maximum differences of approximately 15%. For ~~secondary~~

538 ~~inorganic aerosols (~~SIA~~)~~, while the predicted relative changes in their daily average

539 concentrations due to NO_x reductions are quite similar, very large differences of up to 30%

540 occur for VOC reductions. Sometimes even the direction of change (i.e., increase or decrease)
541 is different. For the oxidants OH and NO_3 radicals, the uncertainties in the relative changes due
542 to emission changes are even larger among different inventory-mechanism combinations,
543 sometimes by as much as 200%. Our results suggest that while the O_3-8h responses to emission
544 changes are not sensitive to the choice of chemical mechanism and emission inventories, using
545 a single model and mechanism to evaluate the effectiveness of emission controls on SIA and
546 atmospheric oxidation capacity may have large errors. For these species, the evaluation of the
547 control strategies may require an ensemble approach with multiple inventories and mechanisms.
548

549 **Data availability**. The dataset for this paper is available upon request from the corresponding
550 author (qying@ust.hk).

551 **Author contributions.** QY designed the study. QY and MJK developed the CMAQ model.
552 MJK conducted the simulations, analyzed the data, and wrote the manuscript. All coauthors
553 contributed to the discussion and revision of the paper.

554 **Competing interests**. The authors declare that they have no conflict of interest.

555 **Acknowledgments**

556 This work was partly supported by the National Natural Science Foundation of China (No.
557 42307142).

References

Akimoto, H., Ohara, T., Kurokawa, J., and Horii, N.: Verification of energy consumption in China during 1996–2003 by using satellite observational data, Atmospheric Environment, 40, 7663–7667, https://doi.org/10.1016/j.atmosenv.2006.07.052, 2006.

Boylan, J. W. and Russell, A. G.: PM and light extinction model performance metrics, goals, and criteria for three-dimensional air quality models, Atmospheric Environment, 40, 4946–4959, https://doi.org/10.1016/j.atmosenv.2005.09.087, 2006.

Bray, C. D., Strum, M., Simon, H., Riddick, L., Kosusko, M., Menetrez, M., Hays, M. D., and Rao, V.: An assessment of important SPECIATE profiles in the EPA emissions modeling platform and current data gaps, Atmospheric Environment, 207, 93–104, https://doi.org/10.1016/j.atmosenv.2019.03.013, 2019.

Byun, D. and Schere, K. L.: Review of the Governing Equations, Computational Algorithms, and Other Components of the Models-3 Community Multiscale Air Quality (CMAQ) Modeling System, Applied Mechanics Reviews, 59, 51–77, https://doi.org/10.1115/1.2128636, 2006.

Carter, W. P. L.: Development of a condensed SAPRC-07 chemical mechanism, Atmospheric Environment, 44, 5336–5345, https://doi.org/10.1016/j.atmosenv.2010.01.024, 2010.

Carter, W. P. L.: Development of a database for chemical mechanism assignments for volatile organic emissions, Journal of the Air & Waste Management Association, 65, 1171–1184, https://doi.org/10.1080/10962247.2015.1013646, 2015.

Carter, W. P. L.: Documentation of the SAPRC-18 mechansim, Report to the California Air Resources Board, 2020.

Carter, W. P. L. and Heo, G.: Development of revised SAPRC aromatics mechanisms, Atmos. Environ., 77, 404–414, https://doi.org/10.1016/j.atmosenv.2013.05.021, 2013.

Carter, W. P. L., Jiang, J., Orlando, J. J., and Barsanti, K. C.: Derivation of atmospheric reaction mechanisms for volatile organic compounds by the SAPRC mechanism generation system (MechGen), Atmospheric Chemistry and Physics, 25, 199–242, https://doi.org/10.5194/acp-25-199-2025, 2025.

Du, H., Yan, M., Liu, X., Zhong, Y., Ban, J., Lu, K., and Li, T.: Exposure to Concurrent Heatwaves and Ozone Pollution and Associations with Mortality Risk: A Nationwide Study in China, Environmental Health Perspectives, 132, 047012, https://doi.org/10.1289/EHP13790, 2024.

Elshorbany, Y. F., Kurtenbach, R., Wiesen, P., Lissi, E., Rubio, M., Villena, G., Gramsch, E., Rickard, A. R., Pilling, M. J., and Kleffmann, J.: Oxidation capacity of the city air of Santiago, Chile, Atmospheric Chemistry and Physics, 9, 2257–2273, https://doi.org/10.5194/acp-9-2257-2009, 2009.

Emery, C., Liu, Z., Russell, A. G., Odman, M. T., Yarwood, G., and Kumar, N.: Recommendations on statistics and benchmarks to assess photochemical model performance, Journal of the Air & Waste Management Association, 67, 582–598, https://doi.org/10.1080/10962247.2016.1265027, 2017.

Feng, Z., Xu, Y., Kobayashi, K., Dai, L., Zhang, T., Agathokleous, E., Calatayud, V., Paoletti, E., Mukherjee, A., Agrawal, M., Park, R. J., Oak, Y. J., and Yue, X.: Ozone pollution threatens the production of major staple crops in East Asia, Nat Food, 3, 47–56, https://doi.org/10.1038/s43016-021-00422-6, 2022.

Finlayson-Pitts, B. J. and Pitts Jr, J. N.: Chemistry of the upper and lower atmosphere: theory, experiments, and applications, Elsevier, 1999.

Geyer, A., Alicke, B., Konrad, S., Schmitz, T., Stutz, J., and Platt, U.: Chemistry and oxidation capacity of the nitrate radical in the continental boundary layer near Berlin, Journal of Geophysical Research: Atmospheres, 106, 8013–8025, https://doi.org/10.1029/2000JD900681, 2001.

Ghude, S. D., Chate, D. M., Jena, C., Beig, G., Kumar, R., Barth, M. C., Pfister, G. G., Fadnavis, S., and Pithani, P.: Premature mortality in India due to PM2.5 and ozone exposure, Geophysical Research Letters, 43, 4650–4658, https://doi.org/10.1002/2016GL068949, 2016.

Griffith, S. M., Hansen, R. F., Dusanter, S., Michoud, V., Gilman, J. B., Kuster, W. C., Veres, P. R., Graus, M., de Gouw, J. A., Roberts, J., Young, C., Washenfelder, R., Brown, S. S., Thalman, R., Waxman, E., Volkamer, R., Tsai, C., Stutz, J., Flynn, J. H., Grossberg, N., Lefer, B., Alvarez, S. L., Rappenglueck, B., Mielke, L. H., Osthoff, H. D., and Stevens, P. S.: Measurements of hydroxyl and hydroperoxy radicals during CalNex-LA: Model comparisons and radical budgets, Journal of Geophysical Research: Atmospheres, 121, 4211–4232, https://doi.org/10.1002/2015JD024358, 2016.

Hu, J., Li, X., Huang, L., Ying, Q., Zhang, Q., Zhao, B., Wang, S., and Zhang, H.: Ensemble prediction of air quality using the WRF/CMAQ model system for health effect studies in China, Atmospheric Chemistry and Physics, 17, 13103–13118, https://doi.org/10.5194/acp-17-13103-2017, 2017a.

Hu, J., Huang, L., Chen, M., Liao, H., Zhang, H., Wang, S., Zhang, Q., and Ying, Q.: Premature Mortality Attributable to Particulate Matter in China: Source Contributions and Responses to Reductions, Environ. Sci. Technol., 51, 9950–9959, https://doi.org/10.1021/acs.est.7b03193, 2017b.

Jiang, J., Carter, W. P. L., Cocker, D. R. I., and Barsanti, K. C.: Development and Evaluation of a Detailed Mechanism for Gas-Phase Atmospheric Reactions of Furans, ACS Earth Space Chem., 4, 1254–1268, https://doi.org/10.1021/acsearthspacechem.0c00058, 2020.

Kang, M., Zhang, J., Zhang, H., and Ying, Q.: On the Relevancy of Observed Ozone Increase during COVID-19 Lockdown to Summertime Ozone and PM2.5 Control Policies in China, Environ. Sci. Technol. Lett., 8, 289–294, https://doi.org/10.1021/acs.estlett.1c00036, 2021.

Kang, M., Hu, J., Zhang, H., and Ying, Q.: Evaluation of a highly condensed SAPRC chemical mechanism and two emission inventories for ozone source apportionment and emission control strategy assessments in China, Science of The Total Environment, 813, 151922, https://doi.org/10.1016/j.scitotenv.2021.151922, 2022.

Kang, M., Zhang, H., and Ying, Q.: Enhanced summertime background ozone by anthropogenic emissions – Implications on ozone control policy and health risk assessment, Atmospheric Environment, 314, 120116, https://doi.org/10.1016/j.atmosenv.2023.120116, ~~2023~~2023a.

Kang, M., Zhang, H., and Ying, Q.: Enhanced summertime background ozone by anthropogenic emissions – Implications on ozone control policy and health risk assessment, Atmospheric Environment, 120116, https://doi.org/10.1016/j.atmosenv.2023.120116, 2023b.

Kim, Y., Sartelet, K., and Seigneur, C.: Comparison of two gas-phase chemical kinetic mechanisms of ozone formation over Europe, J Atmos Chem, 62, 89–119, https://doi.org/10.1007/s10874-009-9142-5, 2009.

Lei, Y., Zhang, Q., He, K. B., and Streets, D. G.: Primary anthropogenic aerosol emission trends for China, 1990–2005, Atmospheric Chemistry and Physics, 11, 931–954, https://doi.org/10.5194/acp-11-931-2011, 2011.

Li, J., Zhang, H., and Ying, Q.: Comparison of the SAPRC07 and SAPRC99 photochemical mechanisms during a high ozone episode in Texas: Differences in concentrations, OH budget and relative response factors, Atmospheric Environment, 54, 25–35, https://doi.org/10.1016/j.atmosenv.2012.02.034, 2012.

Li, K., Jacob, D. J., Liao, H., Shen, L., Zhang, Q., and Bates, K. H.: Anthropogenic drivers of 2013–2017 trends in summer surface ozone in China, Proc Natl Acad Sci USA, 116, 422–427, https://doi.org/10.1073/pnas.1812168116, 2019.

Li, K., Zhang, X., Zhao, B., Bloss, W. J., Lin, C., White, S., Yu, H., Chen, L., Geng, C., Yang, W., Azzi, M., George, C., and Bai, Z.: Suppression of anthropogenic secondary organic aerosol formation by isoprene, npj Clim Atmos Sci, 5, 1–9, https://doi.org/10.1038/s41612-022-00233-x, 2022a.

Li, M., Zhang, Q., Streets, D. G., He, K. B., Cheng, Y. F., Emmons, L. K., Huo, H., Kang, S. C., Lu, Z., Shao, M., Su, H., Yu, X., and Zhang, Y.: Mapping Asian anthropogenic emissions of non-methane volatile organic compounds to multiple chemical mechanisms, Atmospheric Chemistry and Physics, 14, 5617–5638, https://doi.org/10.5194/acp-14-5617-2014, 2014.

Li, N., He, Q., Greenberg, J., Guenther, A., Li, J., Cao, J., Wang, J., Liao, H., Wang, Q., and Zhang, Q.: Impacts of biogenic and anthropogenic emissions on summertime ozone formation in the Guanzhong Basin, China, Atmospheric Chemistry and Physics, 18, 7489–7507, https://doi.org/10.5194/acp-18-7489-2018, 2018.

671   Li, Q., Jiang, J., Afreh, I. K., Barsanti, K. C., and Cocker III, D. R.: Secondary organic aerosol
672   formation from camphene oxidation: measurements and modeling, Atmospheric Chemistry
673   and Physics, 22, 3131–3147, https://doi.org/10.5194/acp-22-3131-2022, 2022b.

674   Liu, T., Hong, Y., Li, M., Xu, L., Chen, J., Bian, Y., Yang, C., Dan, Y., Zhang, Y., Xue, L., Zhao, M.,
675   Huang, Z., and Wang, H.: Atmospheric oxidation capacity and ozone pollution mechanism in
676   a coastal city of southeastern China: analysis of a typical photochemical episode by an
677   observation-based model, Atmospheric Chemistry and Physics, 22, 2173–2190,
678   https://doi.org/10.5194/acp-22-2173-2022, 2022.

679   Lu, X., Hong, J., Zhang, L., Cooper, O. R., Schultz, M. G., Xu, X., Wang, T., Gao, M., Zhao, Y.,
680   and Zhang, Y.: Severe surface ozone pollution in China: A global perspective, Environmental
681   Science & Technology Letters, 5, 487–494, 2018.

682   Lu, X., Zhang, L., Wang, X., Gao, M., Li, K., Zhang, Y., Yue, X., and Zhang, Y.: Rapid Increases in
683   Warm-Season Surface Ozone and Resulting Health Impact in China Since 2013, Environ. Sci.
684   Technol. Lett., 7, 240–247, https://doi.org/10.1021/acs.estlett.0c00171, 2020.

685   Luhar, A. K., Galbally, I. E., Woodhouse, M. T., and Thatcher, M.: An improved
686   parameterisation of ozone dry deposition to the ocean and its impact in a global climate–
687   chemistry model, Atmos. Chem. Phys., 17, 3749–3767, https://doi.org/10.5194/acp-17-
688   3749-2017, 2017.

689   Lyu, X., Li, K., Guo, H., Morawska, L., Zhou, B., Zeren, Y., Jiang, F., Chen, C., Goldstein, A. H.,
690   Xu, X., Wang, T., Lu, X., Zhu, T., Querol, X., Chatani, S., Latif, M. T., Schuch, D., Sinha, V.,
691   Kumar, P., Mullins, B., Seguel, R., Shao, M., Xue, L., Wang, N., Chen, J., Gao, J., Chai, F.,
692   Simpson, I., Sinha, B., and Blake, D. R.: A synergistic ozone-climate control to address
693   emerging ozone pollution challenges, One Earth, 6, 964–977,
694   https://doi.org/10.1016/j.oneear.2023.07.004, 2023.

695   Ma, J. and van Aardenne, J. A.: Impact of different emission inventories on simulated
696   tropospheric ozone over China: a regional chemical transport model evaluation,
697   Atmospheric Chemistry and Physics, 4, 877–887, https://doi.org/10.5194/acp-4-877-2004,
698   2004.

699   Placet, M., Mann, C. O., Gilbert, R. O., and Niefer, M. J.: Emissions of ozone precursors from
700   stationary sources:: a critical review, Atmospheric Environment, 34, 2183–2204,
701   https://doi.org/10.1016/S1352-2310(99)00464-1, 2000.

702   Prinn, R. G.: The Cleansing Capacity of the Atmosphere, Annual Review of Environment and
703   Resources, 28, 29–57, https://doi.org/10.1146/annurev.energy.28.011503.163425, 2003.

704   Real, E., Megaritis, A., Colette, A., Valastro, G., and Messina, P.: Atlas of ozone chemical
705   regimes in Europe, Atmospheric Environment, 320, 120323,
706   https://doi.org/10.1016/j.atmosenv.2023.120323, 2024.

707   Russell, A.: REGIONAL PHOTOCHEMICAL AIR QUALITY MODELING:Model Formulations,
708   History, and State of the Science, Annual Review of Environment and Resources, 22, 537–
709   588, https://doi.org/10.1146/annurev.energy.22.1.537, 1997.

710 Saikawa, E., Kim, H., Zhong, M., Avramov, A., Zhao, Y., Janssens-Maenhout, G., Kurokawa, J.,
711 Klimont, Z., Wagner, F., Naik, V., Horowitz, L. W., and Zhang, Q.: Comparison of emissions
712 inventories of anthropogenic air pollutants and greenhouse gases in China, Atmospheric
713 Chemistry and Physics, 17, 6393–6421, https://doi.org/10.5194/acp-17-6393-2017, 2017.

714 Seinfeld, J. H. and Pandis, S. N.: Atmospheric Chemistry and Physics: From Air Pollution to
715 Climate Change, John Wiley & Sons, 1152 pp., 2016.

716 Sha, Q., Zhu, M., Huang, H., Wang, Y., Huang, Z., Zhang, X., Tang, M., Lu, M., Chen, C., Shi, B.,
717 Chen, Z., Wu, L., Zhong, Z., Li, C., Xu, Y., Yu, F., Jia, G., Liao, S., Cui, X., Liu, J., and Zheng, J.: A
718 newly integrated dataset of volatile organic compounds (VOCs) source profiles and
719 implications for the future development of VOCs profiles in China, Science of The Total
720 Environment, 793, 148348, https://doi.org/10.1016/j.scitotenv.2021.148348, 2021.

721 Silva, S. J. and Heald, C. L.: Investigating Dry Deposition of Ozone to Vegetation, Journal of
722 Geophysical Research: Atmospheres, 123, 559–573,
723 https://doi.org/10.1002/2017JD027278, 2018.

724 Streets, D. G., Bond, T. C., Carmichael, G. R., Fernandes, S. D., Fu, Q., He, D., Klimont, Z.,
725 Nelson, S. M., Tsai, N. Y., Wang, M. Q., Woo, J.-H., and Yarber, K. F.: An inventory of gaseous
726 and primary aerosol emissions in Asia in the year 2000, Journal of Geophysical Research:
727 Atmospheres, 108, https://doi.org/10.1029/2002JD003093, 2003.

728 Wang, C., Huang, X.-F., Han, Y., Zhu, B., and He, L.-Y.: Sources and Potential Photochemical
729 Roles of Formaldehyde in an Urban Atmosphere in South China, Journal of Geophysical
730 Research: Atmospheres, 122, 11,934-11,947, https://doi.org/10.1002/2017JD027266, 2017.

731 Wang, P., Ying, Q., Zhang, H., Hu, J., Lin, Y., and Mao, H.: Source apportionment of
732 secondary organic aerosol in China using a regional source-oriented chemical transport
733 model and two emission inventories, Environmental Pollution, 237, 756–766,
734 https://doi.org/10.1016/j.envpol.2017.10.122, 2018.

735 West, J. J., Fiore, A. M., Horowitz, L. W., and Mauzerall, D. L.: Global health benefits of
736 mitigating ozone pollution with methane emission controls, Proceedings of the National
737 Academy of Sciences of the United States of America, 103, 3988,
738 https://doi.org/10.1073/pnas.0600201103, 2006.

739 Wiedinmyer, C., Akagi, S. K., Yokelson, R. J., Emmons, L. K., Al-Saadi, J. A., Orlando, J. J., and
740 Soja, A. J.: The Fire INventory from NCAR (FINN): a high resolution global model to estimate
741 the emissions from open burning, Geoscientific Model Development, 4, 625–641,
742 https://doi.org/10.5194/gmd-4-625-2011, 2011.

743 Wu, R. and Xie, S.: Spatial Distribution of Ozone Formation in China Derived from Emissions
744 of Speciated Volatile Organic Compounds, Environ. Sci. Technol., 51, 2574–2583,
745 https://doi.org/10.1021/acs.est.6b03634, 2017.

746 Xue, T., Zheng, Y., Geng, G., Xiao, Q., Meng, X., Wang, M., Li, X., Wu, N., Zhang, Q., and Zhu,
747 T.: Estimating Spatiotemporal Variation in Ambient Ozone Exposure during 2013–2017

748 Using a Data-Fusion Model, Environ. Sci. Technol., 54, 14877–14888,
749 https://doi.org/10.1021/acs.est.0c03098, 2020.

750 Yamaji, K., Ohara, T., Uno, I., Kurokawa, J., Pochanart, P., and Akimoto, H.: Future prediction
751 of surface ozone over east Asia using models-3 community multiscale air quality modeling
752 system and regional emission inventory in Asia, Journal of Geophysical Research:
753 Atmospheres, 113, 2008.

754 Yang, Z., Cheng, H. R., Wang, Z. W., Peng, J., Zhu, J. X., Lyu, X. P., and Guo, H.: Chemical
755 characteristics of atmospheric carbonyl compounds and source identification of
756 formaldehyde in Wuhan, Central China, Atmospheric Research, 228, 95–106,
757 https://doi.org/10.1016/j.atmosres.2019.05.020, 2019.

758 Zhang, H., Li, J., Ying, Q., Guven, B. B., and Olaguer, E. P.: Source apportionment of
759 formaldehyde during TexAQS 2006 using a source-oriented chemical transport model,
760 Journal of Geophysical Research: Atmospheres, 118, 1525–1535,
761 https://doi.org/10.1002/jgrd.50197, 2013.

762 Zhang, K., Duan, Y., Huo, J., Huang, L., Wang, Y., Fu, Q., Wang, Y., and Li, L.: Formation
763 mechanism of HCHO pollution in the suburban Yangtze River Delta region, China: A box
764 model study and policy implementations, Atmospheric Environment, 267, 118755,
765 https://doi.org/10.1016/j.atmosenv.2021.118755, 2021.

766
767
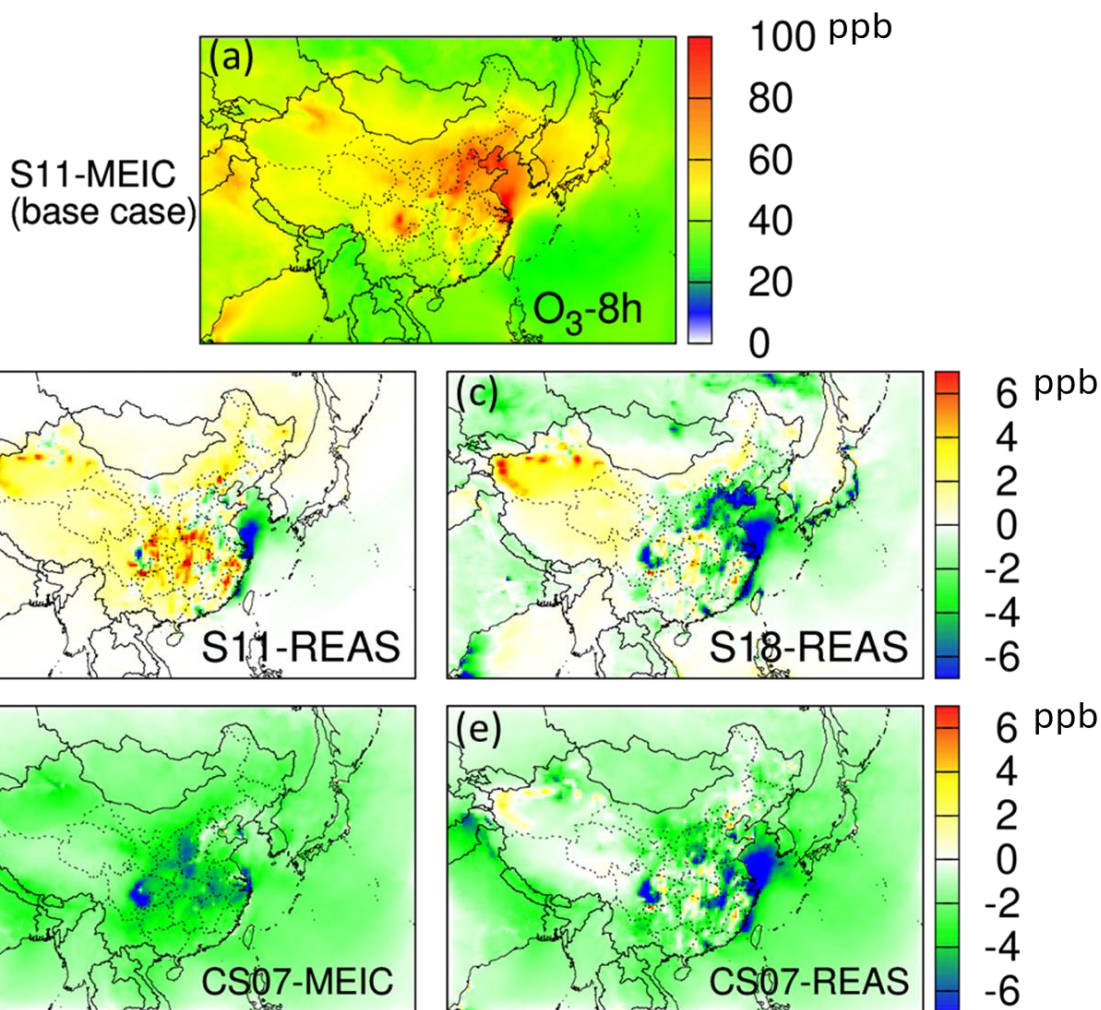
Figure 1. Predicted monthly averages of MDA8 O_3 (O_3-8h) concentrations in July 2017 using (a) the S11 mechanism and MEIC emission inventory (base case), and the differences between the base case and cases using alternative photochemical mechanisms and emission inventories (alternative case – base case): (b) S11 and REAS, (c) S18 and REAS, (d) CS07 and MEIC, and (e) CS07 and REAS inventories. Units are ppb.
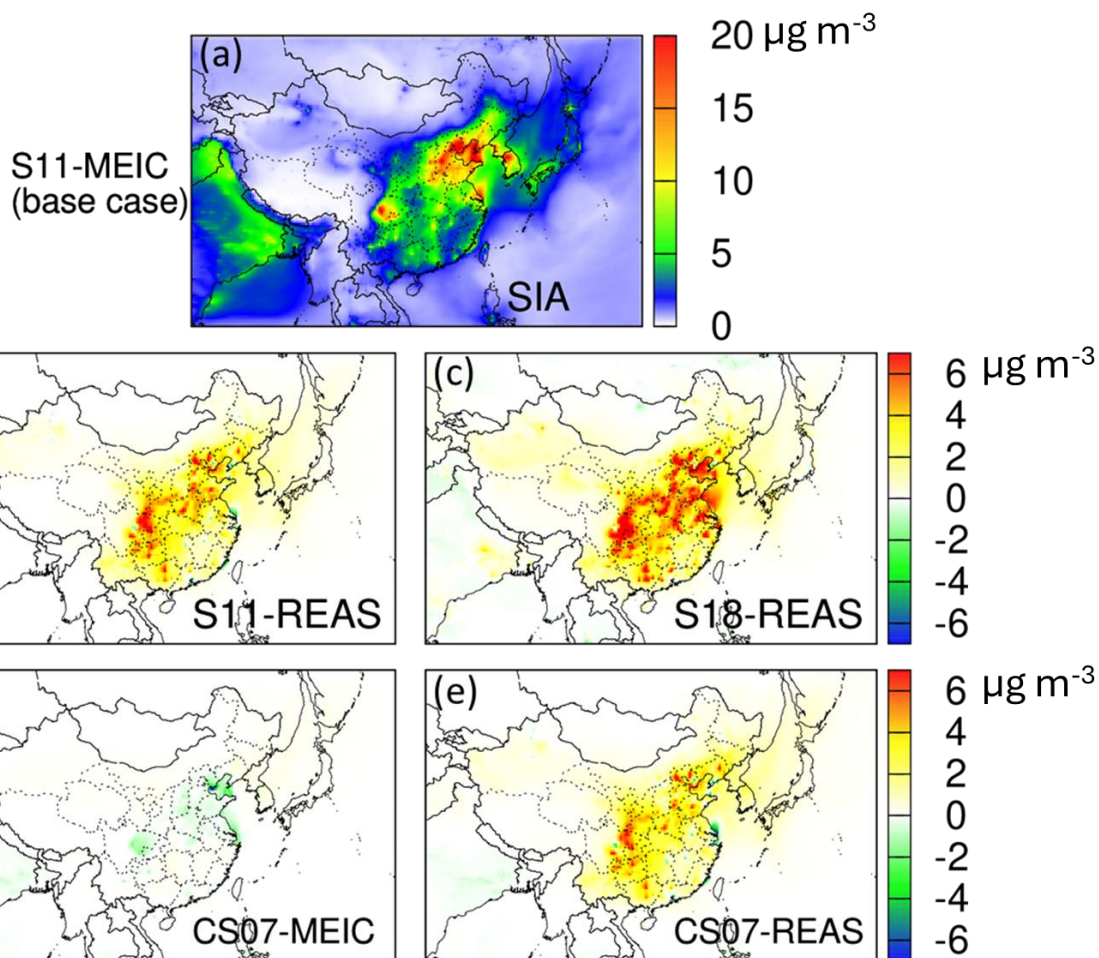
Figure 2. Predicted monthly averages of secondary inorganic aerosol (the sum of nitrate, sulfate and ammonium ion, SIA) concentrations in July 2017 using (a) the S11 mechanism and MEIC emission inventory (base case), and the differences between base case and cases using other photochemical mechanisms and emission inventories (alternative case – base case): (b) S11 and REAS, (c) S18 and REAS, (d) CS07 and MEIC, and (e) CS07 and REAS. Units are $\mu g\ m^{-3}$.
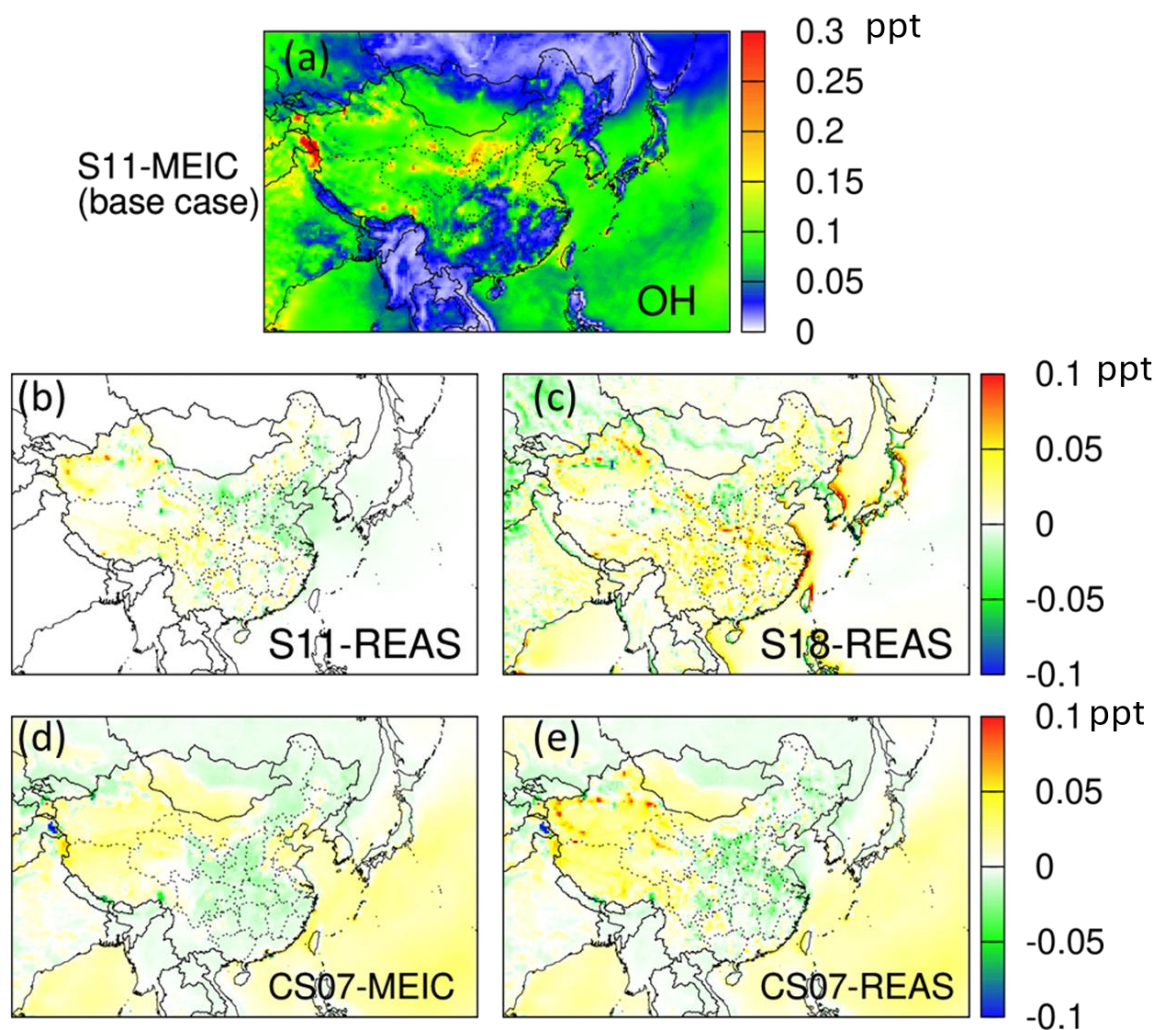
Figure 3. Predicted monthly averages of OH radical concentrations in July 2017 using (a) the S11 mechanism and MEIC emission inventory (base case), and the differences between the base case and cases using other photochemical mechanisms and emission inventories (alternative case – base case): (b) S11 and REAS, (c) S18 and REAS, (d) CS07 and MEIC, and (e) CS07 and REAS. Units are ppt. (0.1 ppt ~ 2.46×10^6 molec cm^{-3})
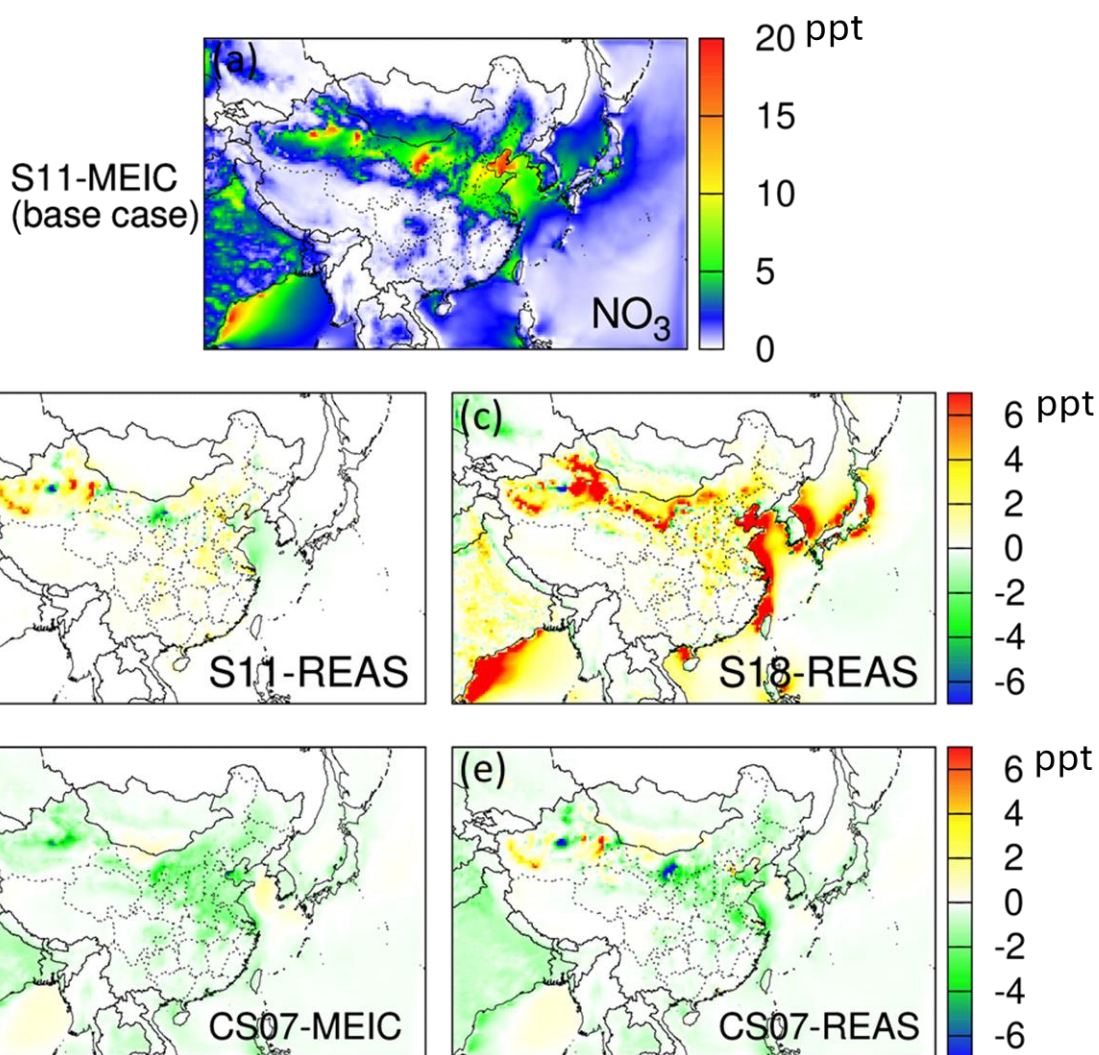
Figure 4. Predicted monthly averages of NO_3 radical concentrations in July 2017 using (a) the S11 mechanism and MEIC emission inventory (base case), and the differences between the base case and cases using alternative photochemical mechanisms and emission inventories (alternative case – base case): (b) S11 and REAS, (c) S18 and REAS, (d) CS07 and MEIC, and (e) CS07 and REAS. Units are in ppt. (0.1 ppt ~ 2.46×10^6 molec cm^{-3})
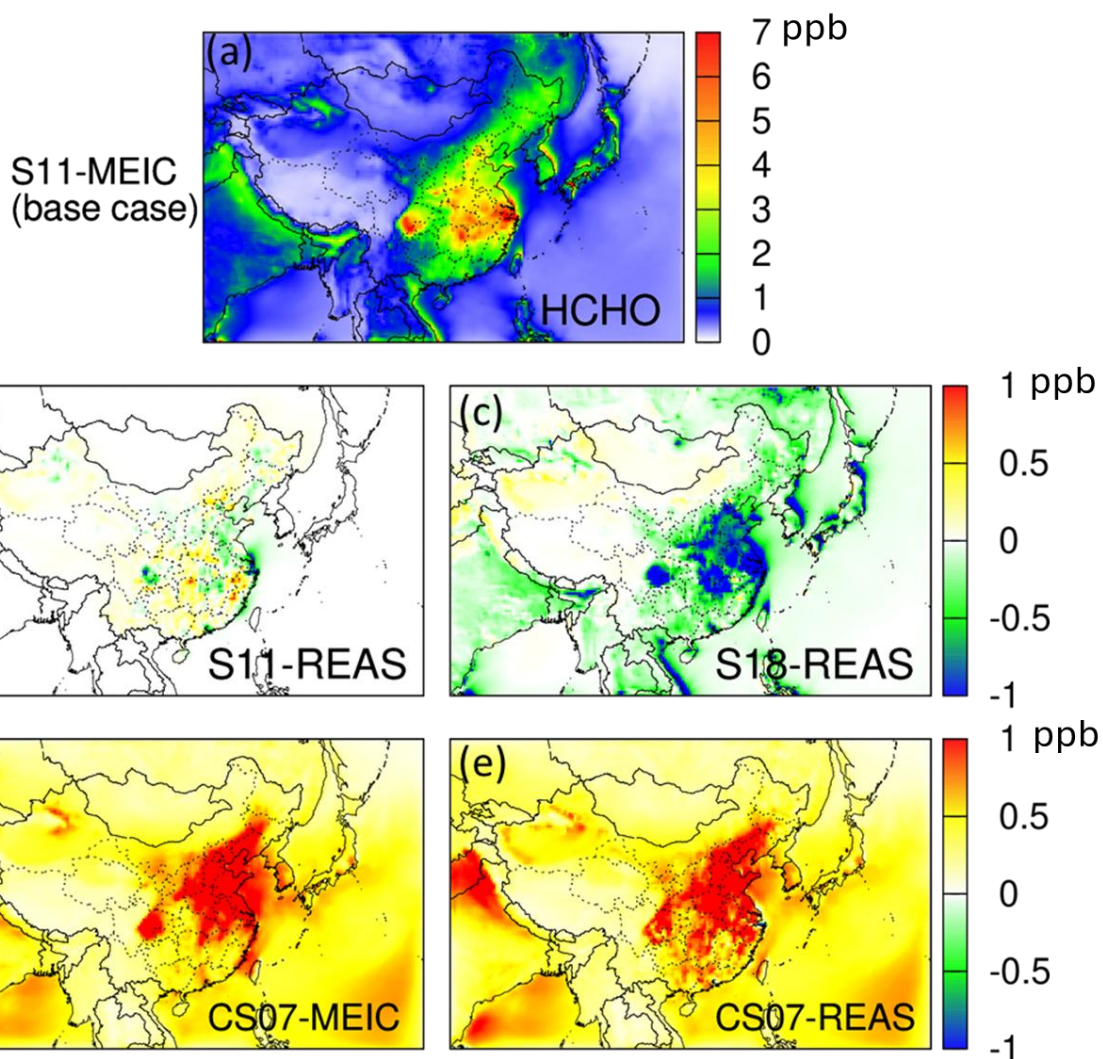
Figure 5. Predicted monthly averages of HCHO concentrations in July 2017 using (a) the S11 mechanism and MEIC emission inventory (base case), and the differences between the base case and cases using alternative photochemical mechanisms and emission inventories (alternative case – base case): (b) S11 and REAS, (c) S18 and REAS, (d) CS07 and MEIC, and (e) CS07 and REAS. Units are ppb.

807
808
809
810
811
812
813
814
815
816
817
818
819
820
821
822
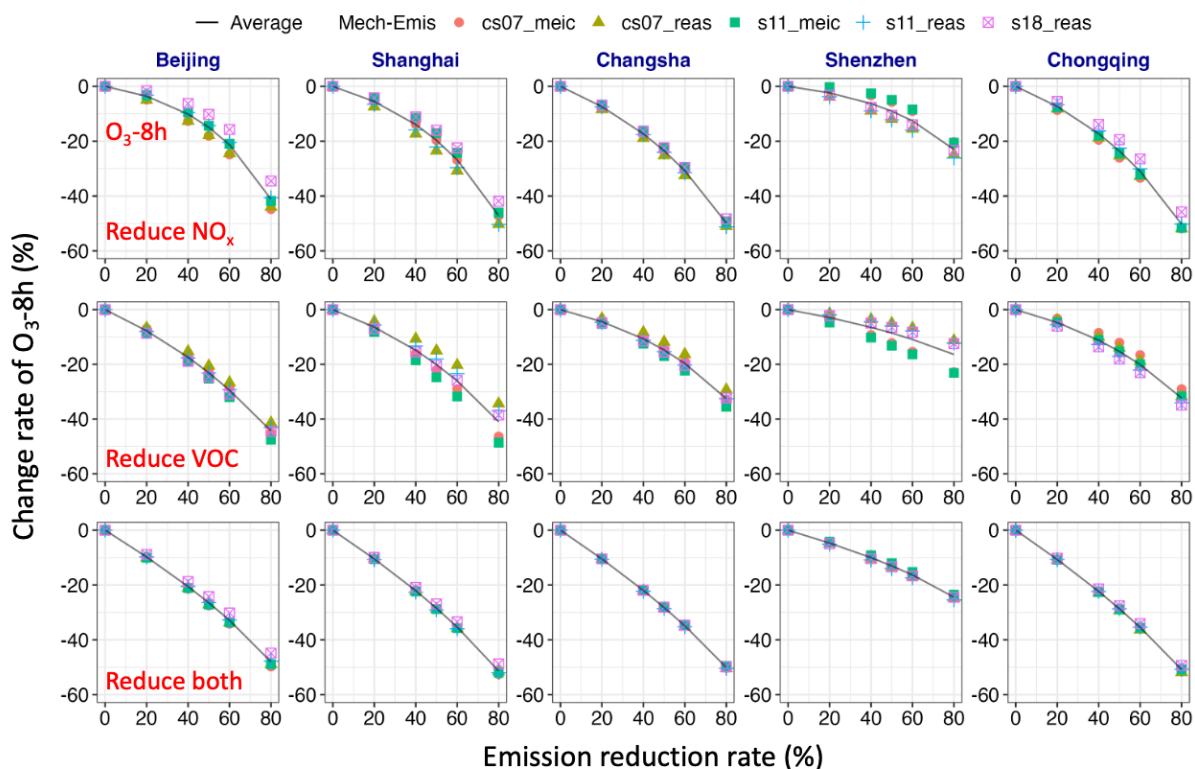
Figure 6. Predicted changes of monthly average MDA8 O_3 (O_3-8h) concentrations in July 2017 due to reductions of NO_x only (first row), VOCs only (second row), and NO_x and VOCs (third row) using different photochemical mechanisms and emission inventories. The black line represents the average change across all mechanisms and inventories at different levels of emission reductions.

827
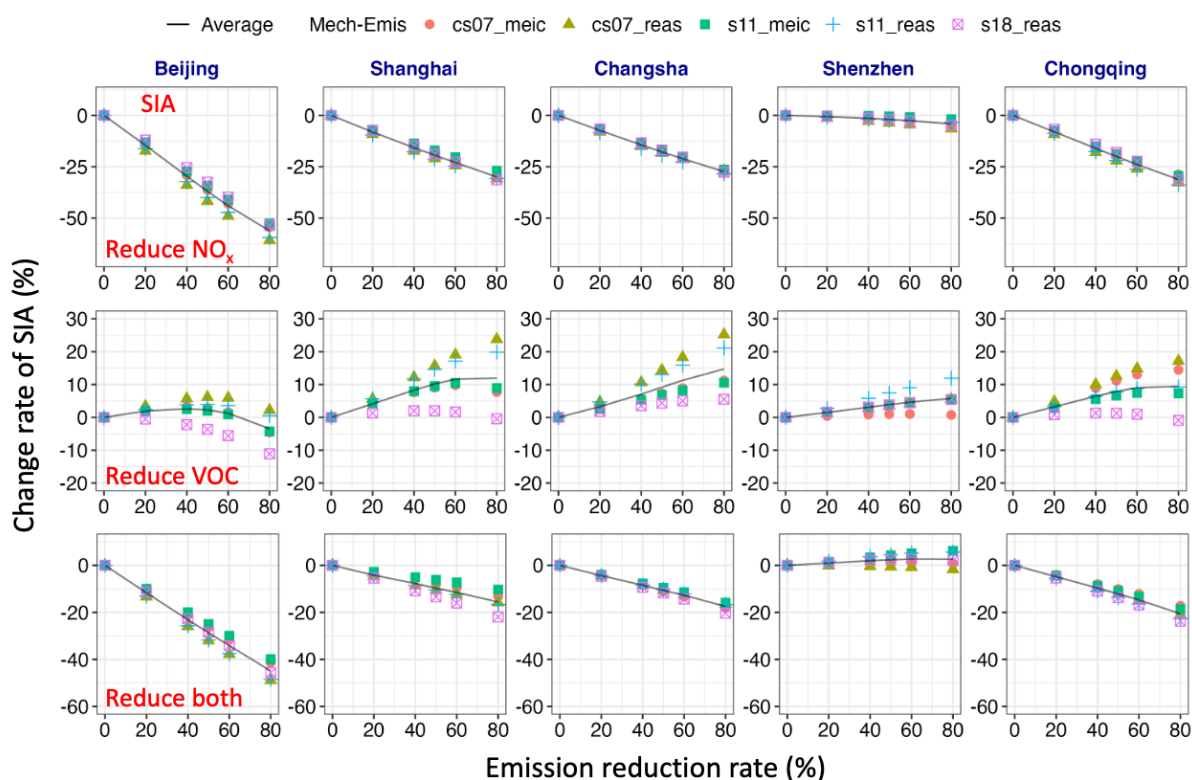
Figure 7. Predicted changes of monthly average secondary inorganic aerosol (nitrate, sulfate, and ammonium, SIA) concentrations in July 2017 due to reductions of NO$_x$ only (first row), VOCs only (second row), and NO$_x$ and VOCs (third row) using different photochemical mechanisms and emission inventories. The black line represents the average change across all mechanisms and inventories at different levels of emission reductions.
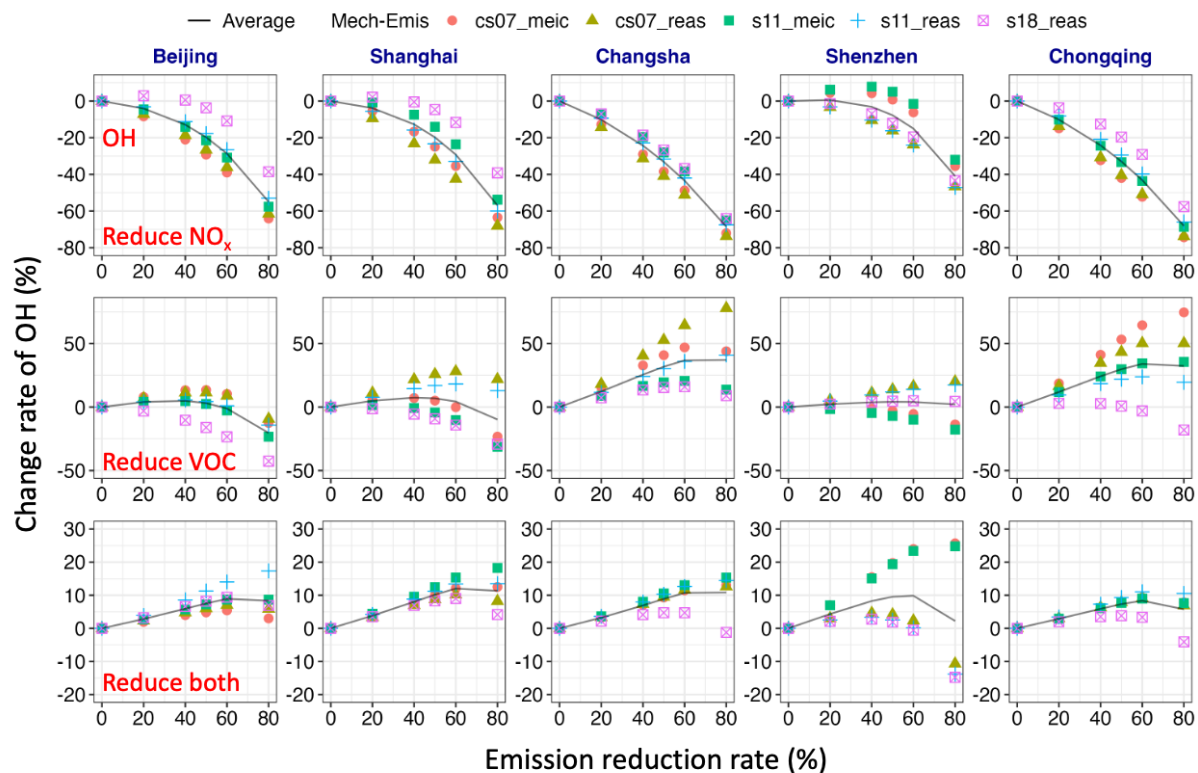
Figure 8. Predicted changes of monthly average OH radical concentrations in July 2017 due to reductions of NO$_x$ only (first row), VOCs only (second row), and NO$_x$ and VOCs (third row) using different photochemical mechanisms and emission inventories. The black line represents the average change across all mechanisms and inventories at different levels of emission reductions.
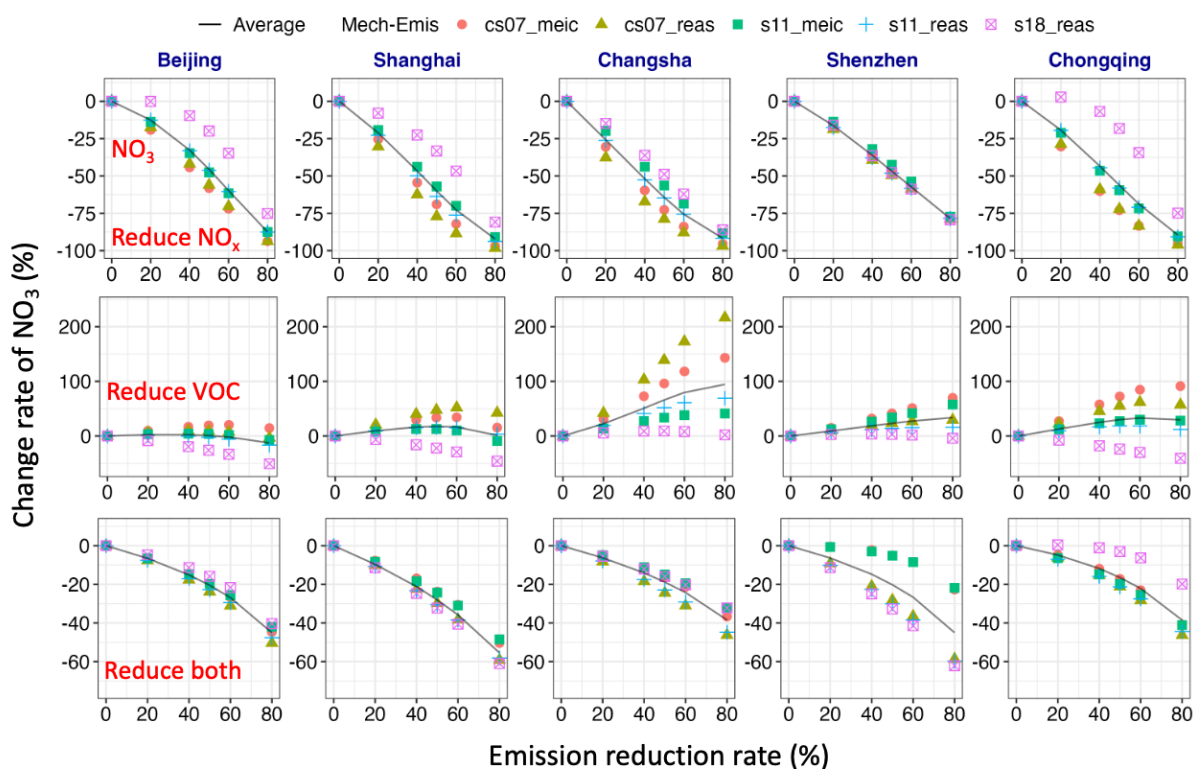
Figure 9. Predicted changes of monthly average NO_3 radical concentrations in July 2017 due to reductions of NO_x only (first row), VOCs only (second row), and NO_x and VOCs (third row) using different photochemical mechanisms and emission inventories. The black line represents the average change across all mechanisms and inventories at different levels of emission reductions.
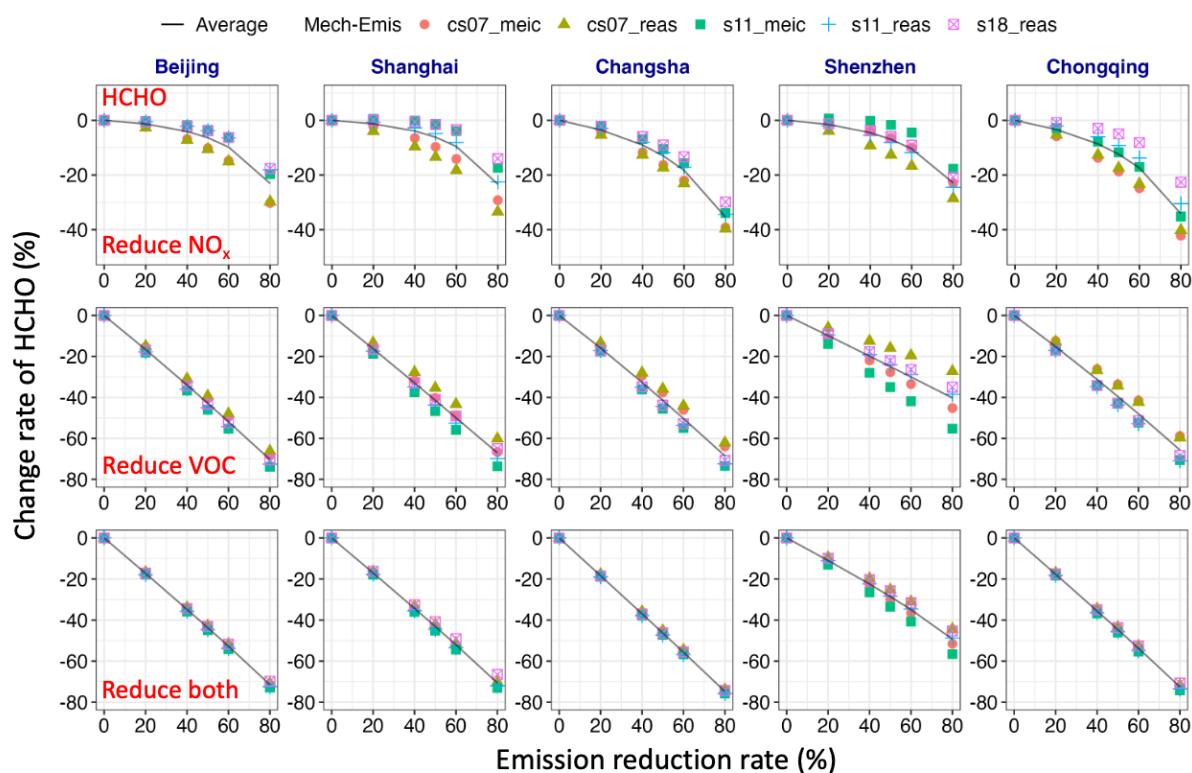
Figure 10. Predicted changes of monthly average HCHO concentrations in July 2017 due to reductions of NO$_x$ only (first row), VOCs only (second row), and NO$_x$ and VOCs (third row) using different photochemical mechanisms and emission inventories. The black line represents the average change across all mechanisms and inventories at different levels of emission reductions.